

This discussion paper is/has been under review for the journal Biogeosciences (BG).  
Please refer to the corresponding final paper in BG if available.

# Identification of two organic bands showing different chemical composition within the skeleton of *Porites lutea*: a confocal Raman microscopy study

M. Wall and G. Nehrke

Alfred Wegener Institute for Polar and Marine Research, Am Handelshafen 12, 27570 Bremerhaven, Germany

Received: 25 June 2012 – Accepted: 26 June 2012 – Published: 10 July 2012

Correspondence to: M. Wall (marlene.wall@awi.de)

Published by Copernicus Publications on behalf of the European Geosciences Union.

**BGD**

9, 8273–8306, 2012

**Different chemical composition within the skeleton of *Porites lutea***

M. Wall and G. Nehrke

Title Page

Abstract

Introduction

Conclusions

References

Tables

Figures

⏪

⏩

◀

▶

Back

Close

Full Screen / Esc

Printer-friendly Version

Interactive Discussion

## Abstract

Confocal Raman microscopy mapping was used to investigate the organic matrix distribution within the skeleton of the coral *Porites lutea*. Two types of growth lines could be identified: one corresponds to the well-known incremental growth layers, whereas the second type of growth lines showed an elemental composition that differed from the incremental growth layers. The position and shape of the latter growth lines resemble either denticle finger-like structures (most likely traces of former spines) or former skeletal surfaces. We hypothesize that these lines are involved in the three-dimensional arrangement of skeletal elements and represent the outer skeletal surface before another growth cycle of elongation, infilling and thickening of skeletal components continues. We show that high spatial resolution mapping can significantly improve our understanding of skeletal growth patterns in coral skeletons.

## 1 Introduction

Scleractinian corals are marine organisms that thrive most vigorously in clear tropical oceans, forming one of the most important marine ecosystems – coral reefs. A thin layer of coral polyps secrete an aragonitic skeleton beneath their basal ectoderm forming an intricate and complex exoskeleton, which represents a chronological layered archive (e.g. Lough and Barnes, 2000; Cohen and McConnaughey, 2003). The fact that environmental information is recorded within these layered structures makes corals an important archive for palaeo climate research. Even though coral reefs have been studied since Darwin's monography (Darwin, 1842) and successfully employed to learn about the past, the fundamental biomineralization processes behind their formation is still not fully understood.

The morphology of skeletal structures of corals represents the foundation of this investigation and will be explained in the following part, followed by a summary of the

**BGD**

9, 8273–8306, 2012

### Different chemical composition within the skeleton of *Porites lutea*

M. Wall and G. Nehrke

Title Page

Abstract

Introduction

Conclusions

References

Tables

Figures

⏪

⏩

◀

▶

Back

Close

Full Screen / Esc

Printer-friendly Version

Interactive Discussion



different biomineralization concepts that have been developed to explain their formation.

Each single polyp consists of different skeletal elements: a columella in the center, septa that radiate away from the center, a wall (theca and epitheca) and dissepiment bordering the corallite to the lateral and basal end, respectively (Sorauf, 1972; Fig. 1). Adjacent corallites either share common walls or, if not, separated corallite walls are connected by skeletal elements forming the coenosteum. All of these macro-morphological elements can be more or less well developed depending on the coral genus (Veron, 2000; Nothurft and Webb, 2007). A close-up of a corallite i.e. viewing individual macro-morphological skeletal elements (such as septa and columella), displays micromorphological features such as spines, granules and nodules, which structure walls, septal margins and septal faces (Sorauf, 1972; Fig. 1). The skeleton of the species studied in this investigation, *Porites lutea*, are relatively porous and less differentiated into macro-morphological elements (Fig. 1) than other species (Sorauf, 1972; Barnes and Devereux, 1988; Nothurft and Webb, 2007). The skeleton is formed of vertical rods (trabeclulae) that are interconnected horizontally by bars called synapticulae or radi and each vertical rod terminates in pali or denticle (Fig. 1a and e) with several spines (Fig. 1c). Both macro- and micro-morphological elements – are composed of two building blocks (microstructural elements) first described by Ogilvie (1896): the centers of calcification (COC) and fibers. The COC – later described as early mineralization zone (EMZ) (Cuif et al., 2004) – build the scaffold for the coral skeleton ultimately responsible for the colony shape, while fibers represent the bulk of the skeleton (e.g. Cohen and McConnaughey, 2003; Nothdurft and Webb, 2007). These different skeletal morphological levels reflect the complex arrangement of coral skeletal elements and it is astonishing how precise they are repeated.

Even though early descriptive studies of coral skeletons focused on the classification of species they also led to the development of biomineralization concepts, of which the first date back to the end of the 19th century (e.g. Pratz, 1882; Stolarski, 2003; Cuif and Dauphin, 2005b). The first biomineralization concepts emphasize the

**BGD**

9, 8273–8306, 2012

## Different chemical composition within the skeleton of *Porites lutea*

M. Wall and G. Nehrke

Title Page

Abstract

Introduction

Conclusions

References

Tables

Figures

⏪

⏩

◀

▶

Back

Close

Full Screen / Esc

Printer-friendly Version

Interactive Discussion

resemblance of microstructural elements as purely inorganic crystals. These growth concepts are based on a simple physico-chemical precipitation process, where centers act as “germs“ and facilitate and direct the growth of aragonite crystals (Bryan and Hill, 1941; Barnes, 1970). Goreau (1959) observed a layer of organic compounds that he interpreted as a template for growth. Young (1971) was one of the first showing that proteins are part of the skeleton. Later scanning electron microscopy (SEM) revealed the incremental growth of coral fibers (Sorauf and Jell, 1977; Cuif and Dauphin, 1998). This insight, together with information from UV-fluorescence examinations, clearly demonstrated microstructural and chemical differences between fibers and centers of calcification (e.g. Cuif and Dauphin, 1998; Cuif et al., 1999). Since then the number of studies that addressed the distribution (Cuif and Dauphin, 1998; Gautret et al., 2000), composition (e.g. Dauphin and Cuif, 1997; Gautret et al., 1997; Puverel et al., 2005) and origin (Clode and Marshall, 2002; Puverel et al., 2005; Tambutte et al., 2007) of organic components within skeletal structures increased rapidly. The incremental growth of coral fibers is expressed in the alternation of organic-rich and organic-depleted growth lines and a layered distribution of trace elements (Meibom et al., 2004, 2007) as well as sulphated polysaccharides. To explain the formation of these layered structures Cuif and Dauphin (2005b) proposed a two-step mode of growth by introducing a sequential process acting at micrometer scale emphasizing an ectodermal control of biomineralization. The ectoderm secretes an organic framework (where sulphated polysaccharides potentially play a major role) onto which minerals grow. The high fluctuation of Mg within fibers (Meibom et al., 2004) suggests that Mg might be incorporated to suppress crystal growth and end the growth cycle (Cuif and Dauphin, 2005b). Stolarski (2003) supported the alternating nature of growth in corals but challenged the proposition of differing temporal formation of EMZ and fibers.

In summary all these observations led to the perception that the formation of a coral skeleton involves the regulative control of dedicated cells/organic molecules during the different stages of growth, rather than “simple inorganic” precipitation of a mineral from a liquid (Cuif and Dauphin, 2005a, b). However, “simple” bio-inorganic models

**BGD**

9, 8273–8306, 2012

**Different chemical composition within the skeleton of *Porites lutea***

M. Wall and G. Nehrke

Title Page

Abstract

Introduction

Conclusions

References

Tables

Figures

⏪

⏩

◀

▶

Back

Close

Full Screen / Esc

Printer-friendly Version

Interactive Discussion



still prevail pointing out the morphological and compositional similarity of abiotic precipitated aragonite under cyclically varying saturation state and pH with skeletal fiber growth of coral microstructural elements (Holcomb et al., 2009). This analogy corresponds to the idea of a liquid filled space between epithelium and skeleton, where supersaturation is maintained to induce crystallization (Furla et al., 2000; Adkins et al., 2003). A critical review of the shortcomings associated with the latter perception can be found in Cuif et al. (2012).

The recent biomineralization concepts explain processes on the micrometer length scale such as growth of fibers around the EMZ. However, they do not provide a linkage to macroscopic structures such as synapticulae joining skeletal elements in regular intervals (Fig. 1) or to temporal differences in formation of different skeletal elements and areas, such as secondary thickening of septa and the formation of dissepiments at the base of the polyp (Nothdurft and Webb, 2007). In coral skeletons, the distribution of the organic matrix – a term encompassing all organic compounds within coral skeletons (Tambutté et al., 2011) – with respect to crystal arrangement has been thoroughly described and attributed a function in calcification (Cuif and Dauphin, 2005b). This skeletal organic matrix was shown to be tightly associated with the mineral phase down to submicrometer scale delineating nano-crystals (Cuif and Dauphin, 2005a; Stolarski and Mazur, 2005) and act as a pre-oriented organic framework that potentially directs the self-assembly of the nano-crystals to form crystal fibers (Cuif and Dauphin, 2005a). Several studies described the different functions for organic compounds extracted from the organic matrix of biominerals. These functions involve mechanisms such as the binding of Ca (Watanabe et al., 2003; Endo et al., 2004), stabilization of amorphous calcium carbonate (Addadi et al., 2003) or inhibition of growth (Wheeler and Sikes, 1984; Marin et al., 1996). According to Cuif et al. (2011, p. 177) “present knowledge of the distribution of organic compounds at the submicrometer scale completely refutes any (...) accidental inclusion of organic compounds within skeletons”. However, the exact function on site within the skeleton and the role in the formation

## Different chemical composition within the skeleton of *Porites lutea*

M. Wall and G. Nehrke

Title Page

Abstract

Introduction

Conclusions

References

Tables

Figures

⏪

⏩

◀

▶

Back

Close

Full Screen / Esc

Printer-friendly Version

Interactive Discussion



of different structural elements (and potentially the three-dimensional arrangement of macromorphological skeletal elements) is still elusive.

The high spatial resolution (sub-micrometer scale) of Confocal Raman Microscopy (CRM), has been demonstrated to be ideal to describe the structural relation between organic and inorganic phases in biogenic materials (e.g. Hild et al., 2008; Nehrke and Nouet, 2011; Neues et al., 2011; Nehrke et al., 2012). Recently, one study (Zhang et al., 2011) used CRM to map the skeleton of a blue coral (*Helipora coerulea*, Octocorallia). They mapped a small region providing a preliminary insight into the ability of CRM to relate the distribution of organic compounds to the mineral phase in coral skeletons. In this study we applied CRM in combination with Polarized Light Microscopy (PLM), SEM and Electron Micro Probe mapping (EMP) to the scleractinian coral species *Porites lutea* (Milne Edwards and Haime, 1860. The main focus was the organic matrix distribution in relation to the mineral phase, in particular the organic-rich (ORGL) and organic-depleted (ODGL) growth lines (as first described in Cuif and Dauphin 1998) that form a growth layer (the so-called environment recording unit as described by e.g. Cuif and Dauphin 2005a) and how they correlate with the distribution of the elements Sr, Mg, and S. Furthermore it should be investigated how the information obtained by CRM can be compared to the information obtained by long established methods like PLM and SEM.

## 2 Material and methods

### 2.1 Coral sample

The scleractinian coral *Porites lutea* (Milne Edwards and Haime, 1860) was collected by SCUBA divers from an off-shore island in the Andaman Sea, Thailand in March 2011. Coral tissue was removed by submerging the specimen in a 5% sodium hypochlorite solution for 24 h, and subsequently rinsing with de-ionised water and drying at 60 °C for 24 h.

**BGD**

9, 8273–8306, 2012

## Different chemical composition within the skeleton of *Porites lutea*

M. Wall and G. Nehrke

Title Page

Abstract

Introduction

Conclusions

References

Tables

Figures



Back

Close

Full Screen / Esc

Printer-friendly Version

Interactive Discussion

The flow chart in Fig. 2 provides an overview of samples (with sample ID) derived from this specimen and gives an outline of the preparation and measurements applied. After tissue removal, three longitudinal and one transversal block (Fig. 1) were cut out of the skeleton and all but one of the longitudinal skeletal blocks were embedded in an epoxy resin (Araldite 2020, Huntsmann). All samples were ground using HERMES water grinding papers (in the order P1200, P2400, and P4000) and polished with a Struers diamond suspension of 3  $\mu\text{m}$  and finished with a 0.3  $\mu\text{m}$  aluminum oxide suspension. Each grinding and polishing step was followed by rinsing the sample with de-ionised water as well as a short cleaning using an ultrasonic bath. To determine how the observed structures continue into deeper levels of the skeleton, a vertical skeletal rod (trabeculae) of one sample was mapped by CRM in three different levels. This was done by re-grinding and polishing after each mapping to remove  $\sim 10 \mu\text{m}$  of the sample.

## 2.2 Confocal Raman microscopy

Raman mapping was done using a WITec alpha 300 R (WITec GmbH, Germany) CRM. Scans with a high spatial resolution were performed using a piezoelectric scanner table having a maximum scan range of  $200 \mu\text{m} \times 200 \mu\text{m}$  and a minimum step size of 4 nm lateral and 0.5 nm vertical. An ultra high throughput spectrometer (UHTS 300, WITec, Germany) equipped with an EMCCD camera was used with a grating of 600 grooves  $\text{mm}^{-1}$ , blazed at 500 nm. This set-up allows for a very short integration time (down to a few ms) and a spectral range from 0–3600  $\text{cm}^{-1}$  or 0–4000  $\text{cm}^{-1}$  depending on the wavelength used (532 nm or 488 nm, respectively). The Raman instrument could also be operated as a normal light microscope using transmitted and reflected light and was equipped with a polarizing filter (one before the sample – the polarizer and one after the sample – the analyzer). The analyzer can be used in the range from 500 to 800 nm allowing on the one hand the operation of the microscope for PLM and on the other hand for polarized Raman microscopy (at 532 nm). All Raman maps were obtained using a Nikon 100x (NA = 0.9) objective, with the polarizer

**BGD**

9, 8273–8306, 2012

### Different chemical composition within the skeleton of *Porites lutea*

M. Wall and G. Nehrke

Title Page

Abstract

Introduction

Conclusions

References

Tables

Figures

⏪

⏩

◀

▶

Back

Close

Full Screen / Esc

Printer-friendly Version

Interactive Discussion



set to 0° and the analyzer to 90°. The spectra during mapping were recorded with a step size of 0.5 μm and an integration time of 50 ms or 10 ms for 532 or 488 nm, respectively. Raman measurements of biogenic materials are often hindered by strong fluorescence, which overlay distinct Raman lines. However, as shown by e.g. Nehrke and Nouet (2011) for the shell of the snail *Nerita undata*, fluorescence intensity distribution of a region can be used as a proxy to map organic matrix distribution within biogenic minerals. Thus, we used the spectral range between 2400–2700 cm<sup>-1</sup> to map the fluorescence intensity distribution across the sample. The spectral analysis and image processing was performed using the WITecProject software (version 2.04, WITec GmbH, Germany).

### 2.3 Scanning electron microscopy

Prior to SEM analysis the samples were etched using 0.1 % formic acid and 3 % glutaraldehyd solution for 50 s to make microstructural features visible (Waite and Andersen, 1980; Cuif and Dauphin, 1998; Stolarski, 2003). After etching the sample was air dried, put on aluminum stabs, and sputter-coated using a platinum-gold target. Scanning electron microscopic images were acquired at 10 kV or 15 kV and 1.7 μA filament current using a Philipps XL 30 Environmental Scanning Electron Microscope (ESEM).

### 2.4 Electron microprobe mapping

Electron Micro-Probe mapping (EMP: JXA-8200 JEOL, Geomar) was used to study minor and trace element distribution in relation to the structures determined by CRM. The EMP maps were obtained by wavelength dispersive spectrometry (WDS) mode measuring simultaneously Mg (Ka, TAP), Sr (La, TAP) and S (Ka, PETH). The electron beam was focused to a spot size of 1 μm, accelerating voltage set to 15 kV and beam current to 20 nA. A step size of 1 μm as well as an accumulation time of 20 ms was used and the map was repeated to gather 10 accumulations of the selected area. Standards

**BGD**

9, 8273–8306, 2012

## Different chemical composition within the skeleton of *Porites lutea*

M. Wall and G. Nehrke

Title Page

Abstract

Introduction

Conclusions

References

Tables

Figures

◀

▶

◀

▶

Back

Close

Full Screen / Esc

Printer-friendly Version

Interactive Discussion

(Vulcanic glass – VG-2) were measured before mapping the sample to calculate concentrations of the trace elements.

## 2.5 Linear extension rate and growth layer thickness

The coral colony was stained *in situ* using alizarin red ( $15 \text{ mg l}^{-1}$ , approx. 16 h) three months before collection. Daily growth rates can be calculated from this staining experiment by measuring the distance from the staining line (visible in longitudinal sections cut along the major growth direction of corallites) to the colony outer surface with a caliper and dividing this distance by the number of days between staining and collection. *Porites* skeletons consist of vertical rods (trabeculae) that are built of EMZ and fibers (Fig. 3). The fibers are deposited to both sides of the EMZ and composed of incremental growth layers (Cuif and Dauphin 2005a). The growth layer thickness was measured perpendicular to the outer coral mineralizing epithelium and comprises a pair of an ORGL and ODGL (see Fig. 3). The vertical growth rate (determined from the staining experiment) was compared to growth layer thickness (determined using CRM fluorescence mapping). Differences in vertical and lateral extension rates result from the oblique arrangement of the growth layers with respect to the vertical line of EMZ. Both growth layer thickness and the angle between growth layers were measured in all Raman maps that displayed the alternation of a ORGL and ODGL using the computer program imageJ.

## 3 Results and discussion

### 3.1 Structural sample characterization

The spectroscopic datasets obtained during the different Raman mappings were first analysed for the characteristic Raman peaks of aragonite (Fig. 4) – namely translational mode ( $155 \text{ cm}^{-1}$ ), librational mode ( $208 \text{ cm}^{-1}$ ), in-plane bend ( $710 \text{ cm}^{-1}$ ) and symmetric stretch ( $1085 \text{ cm}^{-1}$ ) (Fig. 4; Bischoff et al., 1985; Urmos et al., 1991). The

**BGD**

9, 8273–8306, 2012

## Different chemical composition within the skeleton of *Porites lutea*

M. Wall and G. Nehrke

Title Page

Abstract

Introduction

Conclusions

References

Tables

Figures

⏪

⏩

◀

▶

Back

Close

Full Screen / Esc

Printer-friendly Version

Interactive Discussion





line. These two together illustrate the stepping growth mode of coral fibers (e.g. Cuif and Dauphin 2005b). The distances of growth layers were measured perpendicular to the growth lines as explained in Sect. 2.5 (indicated by the position of the scale bar within fluorescence maps, e.g. Fig. 6a2) and equals to a distance of  $3.9 \pm 0.2 \mu\text{m}$  (mean  $\pm$  SE;  $n = 18$ ). These layers encompass on average an angle of  $36 \pm 2^\circ$  (mean  $\pm$  SE;  $n = 16$ ) and hence, a growth layer results in a mean vertical extension of  $12 \mu\text{m}$  (see Fig. 3; calculation: growth layer thickness / sin (angle between growth layers / 2)). This vertical extension (often referred to as linear extension) was compared to the mean daily growth rate (in vertical direction) of this specimen of approx.  $30 \mu\text{m day}^{-1}$ . These data suggest that per day 2–3 growth cycles occur. Meibom et al. (2007) compared average linear extension rates to distances between high Mg bands determined by means of nanoSIMS measurements (on *Porites* sp.) and suggested that within a day up to five growth cycles could be deposited. In his measurements, one growth layer was between 2–5  $\mu\text{m}$  wide, thus, both – cyclicity and growth layer thickness correspond to the values obtained in this study. Cuif et al. (2011) obtained 10–15 cycles per week ( $\sim 2$  cycles per day) for *Galaxea fascicularis* from a consecutive calcein staining experiment. Thus, this study and the study by Meibom et al. (2007) observed a slightly higher number of cycles per day for *Porites* spp. than Cuif et al. (2011) for *Galaxea fascicularis*. Nothdurft and Webb (2007) observed that a vertical extension of 384  $\mu\text{m}$  equals to 36  $\mu\text{m}$  in lateral growth by tracking growth lines in a skeletal rod of *Porites lobata*. This vertical distance was deposited within 12 days (derived from mean growth rates for this species; see Nothdurft and Webb 2007) and equals a lateral growth of 3  $\mu\text{m}$  per day. Based on the growth rates determined in this study and the study by Meibom et al. (2007), 3  $\mu\text{m}$  lateral growth corresponds to approximately one growth cycle per day.

The differences in growth cycles per day summarized here could be of various nature: (1) the coral was stressed from the staining process (Thebault et al., 2006; Houlbreque et al., 2009), (2) effect of the nutritional status (Cuif et al., 2011), (3) daily growth cycles are species-specific (Cuif et al., 2011), and/or (4) growth rates could differ depending on the location within the skeleton for which they are determined. However,

## Different chemical composition within the skeleton of *Porites lutea*

M. Wall and G. Nehrke

[Title Page](#)[Abstract](#)[Introduction](#)[Conclusions](#)[References](#)[Tables](#)[Figures](#)[⏪](#)[⏩](#)[◀](#)[▶](#)[Back](#)[Close](#)[Full Screen / Esc](#)[Printer-friendly Version](#)[Interactive Discussion](#)

especially a nonlinear growth rate in lateral and longitudinal direction and/or different growth rates depending on the distance from the EMZ could explain the observed decrease in number of growth cycles when tracing growth lines over larger areas.

Two types of ORGL could be detected in this study, which differ in thickness and intensity. From here on the wide growth lines showing increased fluorescence (indicated by a blue arrow within Raman fluorescence maps; Fig. 5–7) are referred to as ORGL 2 (Fig. 6B2, b) whereas the thinner incremental growth lines are referred to as ORGL 1 (Fig. 6B2, a). It could be shown that the ORGL 2 continue in deeper skeletal layers of a vertical rod (Fig. 8a–c). Moreover, these lines resemble the corals outer surface forming a three-dimensional organic envelope. Within a skeletal rod the location of this growth line is slightly changing (Fig. 8), in particular in regions where other skeletal elements, such as radi or synapticulae arise. Early mineralization zones are known to build the central skeletal framework directing growth. The organic envelopes described here indicate former outer surfaces and could potentially play a role as initiation points for interconnecting skeletal elements where new EMZ are formed.

### 3.3 Correlation between organic matrices and elemental composition

EMP mapping showed that Sr is slightly variable within the sample without a distinct pattern (Fig. 9). On the other hand, the Mg distribution displayed a banding pattern, which correlates with the fluorescence bands determined by CRM (Fig. 9). Mapping of S showed elevated concentrations in the areas representing the EMZ (Fig. 9). These findings qualitatively agree with previous studies (Cuif et al., 2003; Meibom et al., 2004, 2007, 2008), even though the resolution of EMP is not comparable with high-resolution techniques like XANES or nanoSIMS (Cuif et al., 2003; Meibom et al., 2004). Therefore, a cyclic variation of S within fibers could not be resolved in this study.

As described above, two different types of ORGL were identified by CRM (named type one and type two). The ORGL 1 show elevated Mg concentrations whereas the ORGL 2 are depleted in Mg. In general it is assumed that in corals Mg is associated with organic compounds (Finch and Allison, 2008), which often also show increased S

**BGD**

9, 8273–8306, 2012

## Different chemical composition within the skeleton of *Porites lutea*

M. Wall and G. Nehrke

Title Page

Abstract

Introduction

Conclusions

References

Tables

Figures

⏪

⏩

◀

▶

Back

Close

Full Screen / Esc

Printer-friendly Version

Interactive Discussion



concentrations (Cuif et al., 2012). However, the growth lines of type two do not follow this pattern but show decreased Mg concentration and no pattern in S (Fig. 9). The low Mg ORGL 2 most likely correspond to the distinct low Mg lines described by Meibom et al. (2004, their Fig. 2 – *Pavona clavus*; 2007, their Fig. 2 – *Porites* sp.). Therefore, they would represent a structural feature not restricted to the skeleton of *P. lutea*. Cuif and Dauphin (2005b) proposed that Mg incorporation in incremental growth lines (type one) functions to repress growth before another layer is added. The ORGL 2 identified in this study, however, are characterized by a decreased Mg concentration and therewith a potentially different function.

### 3.4 Growth patterns and cyclicity

Nothdurft and Webb (2007) pointed out that adjoining structural elements like dissepiment and septa are formed at different times. This temporal heterogeneity is not taken into account in existing growth models and therefore requires their adaptation above the microstructural level. The temporal heterogeneity in skeletal formation also becomes obvious when trying to track spines along the calice into deeper parts of the skeleton, where it appears that they are not present. Hence, different regulative processes must act to produce the spine-rich distal end of the corallites, the skeletal layer covering spines above dissepiments before the skeleton is cut off from the polyp as well as the formation of synapticulae at a regular interval. Position and shape of the ORGL 2 resemble either denticle finger-like structures, traces of former spines or previous skeletal surfaces. Hence, the ORGL 2 which differs in elemental composition and location compared to previously described ORGL 1 arrangements, could be involved in regulating three-dimensional growth patterns of micro- and macroarchitectural elements. We hypothesize that these ORGL 2 act as an “envelope” representing the outer surface at a certain time of deposition (Fig. 10c), before it becomes overgrown and covered by a next growth cycle. The temporal units 1–3 in Fig. 10c represent different growth cycles with 1 being the oldest and 3 the youngest deposited skeleton. Each growth cycle lasts about two weeks and ends with an ORGL 2 (Fig. 10c). Within

**BGD**

9, 8273–8306, 2012

## Different chemical composition within the skeleton of *Porites lutea*

M. Wall and G. Nehrke

Title Page

Abstract

Introduction

Conclusions

References

Tables

Figures

⏪

⏩

◀

▶

Back

Close

Full Screen / Esc

Printer-friendly Version

Interactive Discussion



---

**Different chemical composition within the skeleton of *Porites lutea***M. Wall and G. Nehrke

---

[Title Page](#)[Abstract](#)[Introduction](#)[Conclusions](#)[References](#)[Tables](#)[Figures](#)[Back](#)[Close](#)[Full Screen / Esc](#)[Printer-friendly Version](#)[Interactive Discussion](#)

this biweekly cycle elongation, infilling between spine tips and thickening of macromorphological elements takes place (Fig. 10d). This periodicity in growth agrees with the growth model proposed by Nothdurft and Webb (2007). They traced a growth band in their study (Nothdurft and Webb 2007; their Figs. 16c and 17b) that resembles the ORGL 2 described in this study (Fig. 10b) with a similar longitudinal extension spanning approx. 12 days of growth. This observation supports the proposed mechanism of a three-dimensional structural regulation by ORGL 2 in *Porites* skeletal growth that follows a biweekly periodicity.

Cyclicity represents an ubiquitous characteristic of coral skeletal formation. The described cycles range from the cm-level displayed by seasonal density bands (e.g. Lough and Barnes, 2000; Fig. 1) down to the  $\mu\text{m}$ -level of daily/sub-daily formation of incremental growth layers (e.g. Meibom et al., 2007). High-resolution proxy studies detected a cyclicity of measured proxy values in the range of weekly to monthly periods (Meibom et al., 2003; Rollion-Bard et al., 2003; Cohen and Sohn, 2004; Allison et al., 2010, 2011). In these studies the proxy relation (e.g. Sr/Ca) did not only depend on the target parameter (e.g.  $T$ ) but was potentially influenced by other parameters like: (1) metabolic changes involving spawning and larval release at a lunar periodicity (Meibom et al., 2003), (2) weekly tidal forcing overlying temperature forcing (Cohen and Sohn, 2004) and (3) a strong bi-weekly periodicity that was hypothesized to result from increased calcification required for the formation of synapticulae (Cohen and Sohn, 2004). The latter corresponds to the biweekly growth bands (ORGL2) described in this study.

### 3.5 Chemical characterization of organic compounds

So far we have used the fluorescence intensity determined by CRM as a “black box” for organic molecules. This concept is sufficient since the scope of this investigation is on structural information of coral skeletons in relation to three-dimensional growth patterns and not the characterization of organic compounds. The emphasis was laid on obtaining Raman maps of high spatial resolution (requiring a hundred thousand spectra per

scan) hence, it was not possible to obtain spectra with high spectral resolution at the same time. However, it should be pointed out that CRM is much more powerful and can deliver more detailed information for the chemical characterization. Most studies that applied CRM on coral skeleton derived single spectra. Their aim was to check for different carbonate polymorphs (with a spectra range up to  $1300\text{ cm}^{-1}$ ; e.g. Cuif and Dauphin, 1998; Clode et al., 2011) and only few studies focused on organic spectral lines (Perrin and Smith, 2007; Zhang et al., 2011). To demonstrate what kind of chemical information can be obtained, we analyzed the spectra of some areas showing increased fluorescence in more detail and compared the spectra to other studies using Raman spectroscopy on biominerals. Spectral lines not attributed to aragonite were detected (Fig. 11) corresponding to asymmetric  $\text{SO}_4^{2-}$  bend ( $646\text{ cm}^{-1}$ , Jolivet et al., 2008; Zhang et al., 2011), Amid III ( $1190\text{--}1310\text{ cm}^{-1}$ , Jolivet et al., 2008; Zhang et al., 2011), CH bands ( $2850\text{--}3080\text{ cm}^{-1}$ , Perrin and Smith, 2007; Jolivet et al., 2008) and OH group ( $3200\text{--}3400\text{ cm}^{-1}$ , Jolivet et al., 2008). However, there are some difficulties associated with Raman spectral studies of biominerals that need to be considered. In biominerals the mineral phase is generally dominating the spectra and to obtain the very weak organic bands, long integration times are necessary. Additionally, such samples often show high fluorescence that can lead to oversaturation of detectors when long integration times are used (which sometimes can be avoided by decreasing the intensity of the laser, which on the other hand also increases the integration time). Contaminations of the sample during sample preparation such as embedding in epoxy resins need to be considered and accounted for. We used non-embedded samples to reproduce banding pattern of skeletal fibers to exclude the possibility that during grinding and polishing abraded material accumulates predominately at the organic layers. Recent studies used Raman spectroscopy to characterize organic matrix in biominerals (Kaczorowska et al., 2003; Perrin and Smith, 2007; Jolivet et al., 2008; Zhang et al., 2008, 2011 Nehrke and Nouet, 2011), but coral Raman spectroscopic analyses covering a spectral region between  $100\text{--}3200\text{ cm}^{-1}$  are quite rare. However, organic compound bands were detected by all studies (Kaczorowska et al., 2003; Perrin and Smith, 2007;

---

**Different chemical composition within the skeleton of *Porites lutea***M. Wall and G. Nehrke

---

[Title Page](#)[Abstract](#)[Introduction](#)[Conclusions](#)[References](#)[Tables](#)[Figures](#)[Back](#)[Close](#)[Full Screen / Esc](#)[Printer-friendly Version](#)[Interactive Discussion](#)

## Different chemical composition within the skeleton of *Porites lutea*

M. Wall and G. Nehrke

Title Page

Abstract

Introduction

Conclusions

References

Tables

Figures



Back

Close

Full Screen / Esc

Printer-friendly Version

Interactive Discussion



Zhang et al., 2011, this study), although, Kaczorowska et al. (2003) compared the Raman spectra of scleractinian corals to pure aragonite and only detected organic bands for precious corals. In contrast, Perrin and Smith (2007, *Lobophyllia corymbosa* and *Leptastrea purpurea*) and this study (*Porites lutea*) both detected organic compounds within scleractinian coral skeletons. In fact, it was demonstrated the ability to observe both differences in quantity (not absolut but relative Fig. 5–7, Jolivet et al., 2008, for otholiths; Nehrke and Nouet, 2011, for molluscs) as well as quality (spatial distribution, Fig. 11a1 and b1, as well Perrin and Smith, 2007) by Raman spectroscopy. These observations have also been derived for other biominerals (Jolivet et al., 2008, for otholiths; Nehrke and Nouet 2011, for gastropods). Zhang et al. (2011) even discussed the potential to retrieve diurnal environmental variability of phosphorus by mapping the intensity distribution of the symmetric P-O stretch. Corals are well known for recording environmental parameter, however, high-resolution analysis revealed some constraints associated with the skeletal structural complexity (e.g. Meibom et al., 2004; Cuif and Dauphin, 2005b; Juillet-Leclerc et al., 2009; Rollion-Bard et al., 2010). Thus, the full capability of CRM to acquire environmental information needs further investigation.

## 4 Conclusions

In the present study we used CRM on *P. lutea* skeleton samples to demonstrated:

1. that two different types of organic-rich growth lines are present. One of these growth lines corresponds to the well known incremental growth lines. In contrast, the second type of organic-rich growth lines showed an elemental composition that differs from the incremental growth lines (low Mg concentration).
2. that mapping by CRM can be used to visualize the differences in crystal orientation, without the necessity to prepare thin sections.
3. that the layered distribution of organic matrices could be shown and simultaneously related to the orientation of fibers.

---

**Different chemical composition within the skeleton of *Porites lutea***M. Wall and G. Nehrke

---

[Title Page](#)[Abstract](#)[Introduction](#)[Conclusions](#)[References](#)[Tables](#)[Figures](#)[Back](#)[Close](#)[Full Screen / Esc](#)[Printer-friendly Version](#)[Interactive Discussion](#)

4. that CRM mapping can provide information on skeletal growth patterns by tracking growth lines within a skeletal rod (in the polished plane as well as in depth). Position and shape of the second type of organic-rich growth line (within the text referred to as ORGL 2) resemble either denticle finger-like structure, traces of former spines or previous skeletal surfaces. Thus, we hypothesize that this growth lines are involved in the three-dimensional arrangement of skeletal macro- to micromorphological elements and represent the outer skeletal surface before another cycle of elongation, infilling and thickening of skeletal components continues.
5. and that Raman spectra of organic compounds can be measured. The latter represents a powerful possibility in the chemical characteriazation of organic compounds wihin coral skeletons.

Hence, high spatial resolution CRM mapping enables to track growth lines over large skeletal areas and relate skeletal enteties (EMZ and incremental growth layer) as well as the organic to the mineral phase. This simultaneously obtained information can definitively deepen our understanding of growth patterns in coral skeletons and improve growth concepts above micrometer scale. Organic compounds are hypothesized to play a crucial role in coral biomineraliatzion. Here we detected an organic-rich growth line that potentially regulates coral growth. EMP maps provided a first indication of how to complement CRM studies and added new information. Instruments of high spatial resolution (e.g. nanoSIMS, or XANES) are crucial in the investigation of biogenic materials but are restricted by the small area that can be mapped. Thus, a combination of these methods with with CRM is highly valueable. CRM allows to identify the area of interest prior to measurements by these methods, which are often difficult to access and are cost intensive.

*Acknowledgements.* The authors thank Jan Fietzke (Geomar) for the assistance with the EMP measurements. This work was supported by the European Commission through grant 211384 (EU FP7 “EPOCA”), the German Federal Ministry of Education and Research (BMBF, FKZ 03F0608, “BIOACID”), and has received funding from the European Community’s Seventh Framework Programme under grant agreement 265103 (Project MedSeA).

## References

- Addadi, L., Raz, S., and Weiner, S.: Taking advantage of disorder: Amorphous calcium carbonate and its roles in biomineralization, *Adv. Mater.*, 15, 959–970, doi:10.1002/adma.200300381, 2003.
- Adkins, J. F., Boyle, E. A., Curry, W. B., and Lutringer, A.: Stable isotopes in deep-sea corals and a new mechanism for “vital effects”, *Geochim. Cosmochim. Ac.*, 67, 1129–1143, 2003.
- Allison, N., Finch, A. A., and EIMF:  $\delta^{11}\text{B}$ , Sr, Mg and B in a modern porites coral: The relationship between calcification site pH and skeletal chemistry, *Geochim. Cosmochim. Ac.*, 74, 1790–1800, doi:10.1016/j.gca.2009.12.030, 2010.
- Allison, N., Cohen, I., Finch, A. A., Erez, J., and EMIF: Controls on Sr/Ca and Mg/Ca in scleractinian corals: The effects of Ca-ATPase and transcellular Ca channels on skeletal chemistry, *Geochim. Cosmochim. Ac.*, 75, 6350–6360, doi:10.1016/j.gca.2011.08.012, 2011.
- Barnes, D. J.: Coral skeletons: an explanation of their growth and structure, *Science*, 170, 1305–1308, 1970.
- Barnes, D. J. and Devereux, M. J.: Variations in skeletal architecture associated with density banding in the hard coral *Porites*, *J. Exp. Mar. Biol. Ecol.*, 121, 37–54, doi:10.1016/0022-0981(88)90022-6, 1988.
- Bischoff, W. D., Sharma, S. K., and Mackenzie, F. T.: Carbonate ion disorder in synthetic and biogenic magnesian calcites: a Raman spectral study, *Am. Mineral.*, 70, 581–589, 1985.
- Bryan, W. and Hill, D.: Spherulitic crystallization as a mechanism of skeletal growth in the hexacorals, *Proc. R. Soc. Queensl.*, 52, 78–91, 1941.
- Clode, P. L. and Marshall, A. T.: Low temperature FESEM of the calcifying interface of a scleractinian coral, *Tissue Cell*, 34, 187–198, doi:10.1016/S0040-8166(02)00031-9, 2002.

**BGD**

9, 8273–8306, 2012

## Different chemical composition within the skeleton of *Porites lutea*

M. Wall and G. Nehrke

Title Page

Abstract

Introduction

Conclusions

References

Tables

Figures

⏪

⏩

◀

▶

Back

Close

Full Screen / Esc

Printer-friendly Version

Interactive Discussion

## Different chemical composition within the skeleton of *Porites lutea*

M. Wall and G. Nehrke

Title Page

Abstract

Introduction

Conclusions

References

Tables

Figures

◀

▶

◀

▶

Back

Close

Full Screen / Esc

Printer-friendly Version

Interactive Discussion

Clode, P. L., Lema, K., Saunders, M., and Weiner, S.: Skeletal mineralogy of newly settling acropora millepora (scleractinia) coral recruits, *Coral Reefs*, 30, 1–8, doi:10.1007/s00338-010-0673-7, 2011.

Cohen, A. L. and McConnaughey, T.: Geochemical perspectives on coral mineralization, in: *Biom mineralization*, edited by: Dove, P. M., Weiner, S., and de Yoreo, J. J., *Reviews in Mineralogy and Geochemistry*, Mineralogical Society of America, 2003.

Cohen, A. L. and Sohn, R. A.: Tidal modulation of Sr/Ca ratios in a Pacific reef coral, *Geophys. Res. Lett.*, 31, L16310, doi:10.1029/2004gl020600, 2004.

Cuif, J.-P. and Dauphin, Y.: Microstructural and physico-chemical characterization of “centers of calcification” in septa of some recent scleractinian corals, *Palaeontol. Z.*, 72, 257–270, 1998.

Cuif, J. P. and Dauphin, Y.: The Environment Recording Unit in coral skeletons – a synthesis of structural and chemical evidences for a biochemically driven, stepping-growth process in fibres, *Biogeosciences*, 2, 61–73, doi:10.5194/bg-2-61-2005, 2005a.

Cuif, J.-P. and Dauphin, Y.: The two-step mode of growth in the scleractinian coral skeletons from the micrometer to the overall scale, *J. Strat. Biol.*, 150, 319–331, 2005b.

Cuif, J. P., Dauphin, Y., and Gautret, P.: Compositional diversity of soluble mineralizing matrices in some recent coral skeletons compared to fine-scale growth structures of fibres: Discussion of consequences for biomineralization and diagenesis, *Int. J. Earth Sci.*, 88, 582–592, doi:10.1007/s005310050286, 1999.

Cuif, J.-P., Dauphin, Y., Doucet, J., Salomé, M., and Susini, J.: XANES mapping of organic sulfate in three scleractinian coral skeletons, *Geochim. Cosmochim. Ac.*, 67, 75–83, 2003.

Cuif, J.-P., Dauphin, Y., Berthet, P., and Jegoudez, J.: Associated water and organic compounds in coral skeletons: quantitative thermogravimetry coupled to infrared absorption spectrometry, *Geochem. Geophys. Geosys.*, 5, doi:10.1029/2004GC000783, 2004.

Cuif, J.-P., Dauphin, Y., and Sorauf, J.: *Biom minerals and fossils through time*, Cambridge University Press, Cambridge, 490 pp., 2011.

Cuif, J.-P., Dauphin, Y., Nehrke, G., Nouet, J., and Perez-Huerta, A.: Layered growth and crystallization in calcareous biom minerals: Impact of structural and chemical evidences on two major concepts in invertebrate biomineralization studies, *Minerals*, 2, 11–39, 2012.

Darwin, C.: *The structure and distribution of coral reef*, University of California Press, London, UK, 1842.



## Different chemical composition within the skeleton of *Porites lutea*

M. Wall and G. Nehrke

Title Page

Abstract

Introduction

Conclusions

References

Tables

Figures

⏪

⏩

◀

▶

Back

Close

Full Screen / Esc

Printer-friendly Version

Interactive Discussion

- Juillet-Leclerc, A., Reynaud, S., Rollion-Bard, C., Cuif, J. P., Dauphin, Y., Blamart, D., Ferrier-Pages, C., and Allemand, D.: Oxygen isotopic signature of the skeletal microstructures in cultured corals: Identification of vital effects, *Geochim. Cosmochim. Ac.*, 73, 5320–5332, doi:10.1016/j.gca.2009.05.068, 2009.
- 5 Kaczorowska, B., Hacura, A., Kupka, T., Wrzalik, R., Talik, E., Pasterny, G., and Matuszewska, A.: Spectroscopic characterization of natural corals, *Anal. Bioanal. Chem.*, 377, 1032–1037, doi:10.1007/s00216-003-2153-1, 2003.
- Lough, J. M. and Barnes, D. J.: Environmental controls on growth of the masisve coral *Porites*, *J. Exp. Mar. Biol. Ecol.*, 245, 225–243, 2000.
- 10 Marin, F., Smith, M., Isa, Y., Muyzer, G., and Westbroek, P.: Skeletal matrices, mucis, and the origin of invertebrate calcification, *P Natl Acad Sci USA*, 93, 1554–1559, doi:10.1073/pnas.93.4.1554, 1996.
- Meibom, A., Stage, M., Wooden, J., Constantz, B. R., Dunbar, R. B., Owen, A., Grumet, N., Bacon, C. R., and Chamberlain, C. P.: Monthly Strontium/Calcium oscillations in symbiotic coral aragonite: Biological effects limiting the precision of the paleotemperature proxy, *Geophys. Res. Lett.*, 30, 1418, doi:10.1029/2002gl016864, 2003.
- 15 Meibom, A., Cuif, J. P., Hillion, F. O., Constantz, B. R., Juillet-Leclerc, A., Dauphin, Y., Watanabe, T., and Dunbar, R. B.: Distribution of magnesium in coral skeleton, *Geophys. Res. Lett.*, 31, L23306, doi:10.1029/2004gl021313, 2004.
- 20 Meibom, A., Mostefaoui, S., Cuif, J.-P., Dauphin, Y., Houlbreque, F., Dunbar, R., and Constantz, B.: Biological forcing controls the chemistry of reef-building coral skeleton, *Geophys. Res. Lett.*, 34, 1–5, 2007.
- Meibom, A., Cuif, J.-P., Houlbreque, F., Mostefaoui, S., Dauphin, Y., Meibom, K. L., and Dunbar, R.: Compositional variations at ultra-structure length scales in coral skeleton, *Geochim. Cosmochim. Acta*, 72, 1555–1569, 2008.
- 25 Nehrke, G. and Nouet, J.: Confocal Raman microscope mapping as a tool to describe different mineral and organic phases at high spatial resolution within marine biogenic carbonates: case study on *Nerita undata* (Gastropoda, Neritopsina), *Biogeosciences*, 8, 3761–3769, doi:10.5194/bg-8-3761-2011, 2011.
- 30 Nehrke, G., Poigner, H., Wilhelms-Dick, D., Brey, T., and Abele, D.: Coexistence of three calcium carbonate polymorphs in the shell of the Antarctic clam *Laternula elliptica*, *Geochem. Geophys. Geosyst.*, 13, Q05014, doi:10.1029/2011gc003996, 2012.

## Different chemical composition within the skeleton of *Porites lutea*

M. Wall and G. Nehrke

Title Page

Abstract

Introduction

Conclusions

References

Tables

Figures

⏪

⏩

◀

▶

Back

Close

Full Screen / Esc

Printer-friendly Version

Interactive Discussion



- Neues, F., Hild, S., Epple, M., Marti, O., and Ziegler, A.: Amorphous and crystalline calcium carbonate distribution in the tergite cuticle of moulting *Porcellio scaber* (Isopoda, Crustacea), *J. Strat. Biol.*, 175, 10–20, doi:10.1016/j.jsb.2011.03.019, 2011.
- 5 Nothdurft, L. D. and Webb, G. E.: Microstructure of common reef-building coral genera *Acropora*, *Pocillopora*, *Goniastrea* and *Porites*: constraints on spatial resolution in geochemical sampling, *Facies*, 53, 1–26, 2007.
- Ogilvie, M.: Microscopic and systematic study of Madreporarian types of corals, *Philos. T. R. Soc. Lond.*, 187, 83–187, 1896.
- 10 Perrin, C. and Smith, D. C.: Earliest steps of diagenesis in living scleractinian corals: evidence from ultrastructural pattern and Raman spectroscopy, *J. Sediment. Res.*, 77, 495–507, 2007.
- Pratz, E.: Über die verwandtschaftlichen Beziehungen einiger Korallengattungen mit hauptsächlichlicher Berücksichtigung ihrer Septalstruktur, *Palaeontographica*, 29, 81–122, 1882.
- 15 Puverel, S., Tambutte, E., Zoccola, D., Domart-Coulon, I., Bouchot, A., Lotto, S., Allemand, D., and Tambutte, S.: Antibodies against the organic matrix in scleractinians: a new tool to study coral biomineralization, *Coral Reefs*, 24, 149–156, doi:10.1007/s00338-004-0456-0, 2005.
- Rollion-Bard, C., Blamart, D., Cuif, J. P., and Dauphin, Y.: In situ measurements of oxygen isotopic composition in deep-sea coral, *Lophelia pertusa*: Re-examination of the current geochemical models of biomineralization, *Geochim. Cosmochim. Ac.*, 74, 1338–1349, doi:10.1016/j.gca.2009.11.011, 2010.
- 20 Sorauf, J.: Skeletal microstructure and microarchitecture in scleractinian (Coelenterata), *Palaeontology*, 15, 88–107, 1972.
- Sorauf, J. and Jell, J. S.: Strucutre and incremental growth in the ahermatypic coral *Desmophyllum cristagalli* from the north Atlantic, *Palaeontology*, 20, 1–19, 1977.
- 25 Stolarski, J.: Three-dimensional micro- and nanostructural characteristics of scleractinian coral skeleton: A biocalcification proxy, *Acta Palaeontol. Pol.*, 48, 497–530, 2003.
- Stolarski, J. and Mazur, M.: Nanostructure of biogenic versus abiogenic calcium carbonate crystals, *Acta Palaeontol. Pol.*, 50, 847–865, 2005.
- Tambutte, E., Allemand, D., Zoccola, D., Meibom, A., Lotto, S., Caminiti, N., and Tambutte, S.: 30 Observations of the tissue-skeleton interface in the scleractinian coral *Stylophora pistillata*, *Coral Reefs*, 26, 517–529, doi:10.1007/s00338-007-0263-5, 2007.

## Different chemical composition within the skeleton of *Porites lutea*

M. Wall and G. Nehrke

Title Page

Abstract

Introduction

Conclusions

References

Tables

Figures

⏪

⏩

◀

▶

Back

Close

Full Screen / Esc

Printer-friendly Version

Interactive Discussion

- Tambutté, S., Holcomb, M., Ferrier-Pagès, C., Reynaud, S., Tambutté, E., Zoccola, D., and Allemand, D.: Coral biomineralization: From the gene to the environment, *J. Exp. Mar. Biol. Ecol.*, 408, 58–78, doi:10.1016/j.jembe.2011.07.026, 2011.
- Thebault, J., Chauvaud, L., Clavier, J., Fichez, R., and Morize, E.: Evidence of a 2-day periodicity of striae formation in the tropical scallop *Comptopallium radula* using calcein marking, *Mar. Biol.*, 149, 257–267, doi:10.1007/s00227-005-0198-8, 2006.
- Urmos, J., Sharma, S. K., and Mackenzie, F. T.: Characterization of some biogenic carbonates with Raman-spectroscopy, *Am. Mineral.*, 76, 641–646, 1991.
- Veron, J. E. N.: Corals of the World, Volume 1, Australian Institute of Marine Science, Townsville, 2000.
- Watanabe, T., Fukuda, I., China, K., and Isa, Y.: Molecular analyses of protein components of the organic matrix in the exoskeleton of two scleractinian coral species, *Comp. Biochem. Physiol. B: Biochem. Mol. Biol.*, 136, 767–774, doi:10.1016/s1096-4959(03)00177-5, 2003.
- Wheeler, A. P. and Sikes, C. S.: Regulation of carbonate calcification by organic matrix, *Am. Zool.*, 24, 933–944, 1984.
- Young, S.: Organic material from scleractinian coral skeletons -I. variation in composition between several species, *Comp. Biochem. Physiol. B: Biochem. Mol. Biol.*, 40, 113–120, 1971.
- Zhang, F., Cai, W., Sun, Z., and Zhang, J.: Regular variations in organic matrix composition of small yellow croaker (*Pseudociaena polyactis*) otoliths: an in situ Raman microspectroscopy and mapping study, *Anal. Bioanal. Chem.*, 390, 777–782, doi:10.1007/s00216-007-1695-z, 2008.
- Zhang, F. F., Cai, W. Y., Zhu, J. C., Sun, Z. R., and Zhang, J.: In Situ Raman Spectral Mapping Study on the Microscale Fibers in Blue Coral (*Heliopora coerulea*) Skeletons, *Anal. Chem.*, 83, 7870–7875, doi:10.1021/ac2017663, 2011.

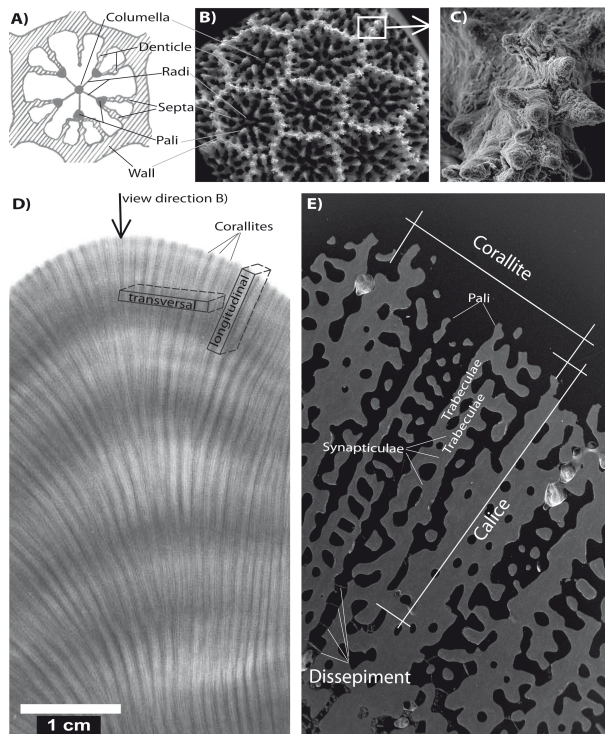


**Fig. 1.** Scanning electron microscopic (SEM) images and X-radiograph positive of *Porites lutea* (Milne Edwards and Haime, 1860). **(A)** Schematic representation of a *Porites* corallite indicating the macromorphological elements. **(B)** Distal view of ceroid corallites. **(C)** Detail showing the spines structuring septal walls. **(D)** X-radiograph of the coral skeleton displaying yearly density banding pattern. Arrow indicates view direction in **(B)** and rectangles show how skeletal blocks were cut out of the skeleton to obtain transversal and longitudinal samples. **(E)** Scanning electron microscopic (SEM) image of a longitudinal section displaying skeletal elements forming the corallite.

**Different chemical composition within the skeleton of *Porites lutea***

M. Wall and G. Nehrke

Title Page

Abstract Introduction

Conclusions References

Tables Figures

◀ ▶

◀ ▶

Back Close

Full Screen / Esc

Printer-friendly Version

Interactive Discussion

Different chemical composition within the skeleton of *Porites lutea*

M. Wall and G. Nehrke

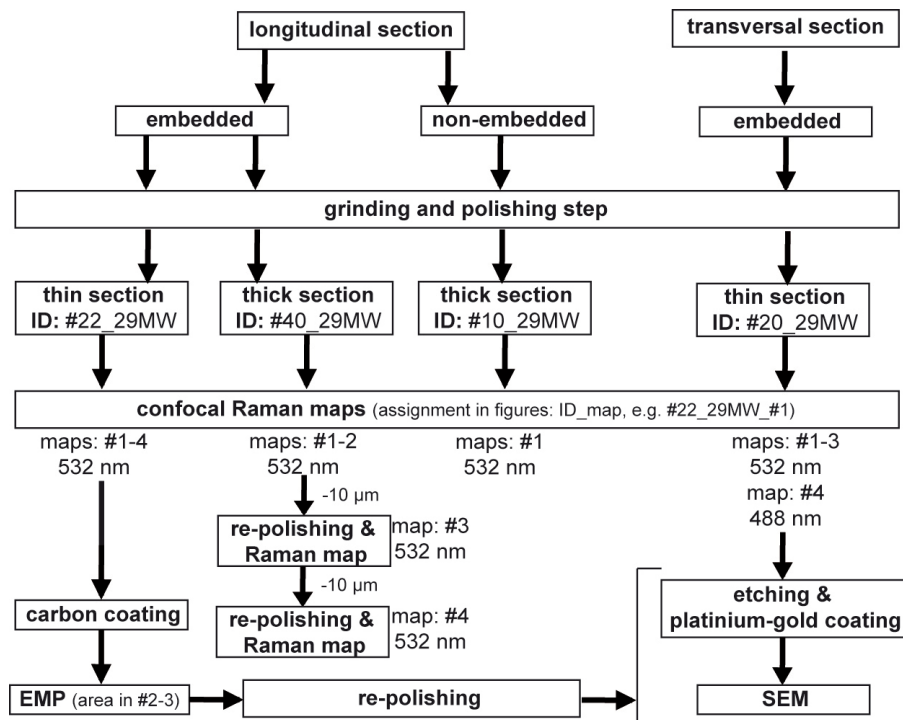


**Fig. 2.** Flow chart displays the chronology of preparation and measurement steps for individual samples (ID). For confocal Raman measurements, the number of maps and laser wavelength used for each map are also given. (Within subsequent figures Raman maps are denoted by: ID\_map, e.g. #22\_29MW\_#1).

Title Page

Abstract Introduction

Conclusions References

Tables Figures

◀ ▶

◀ ▶

Back Close

Full Screen / Esc

Printer-friendly Version

Interactive Discussion



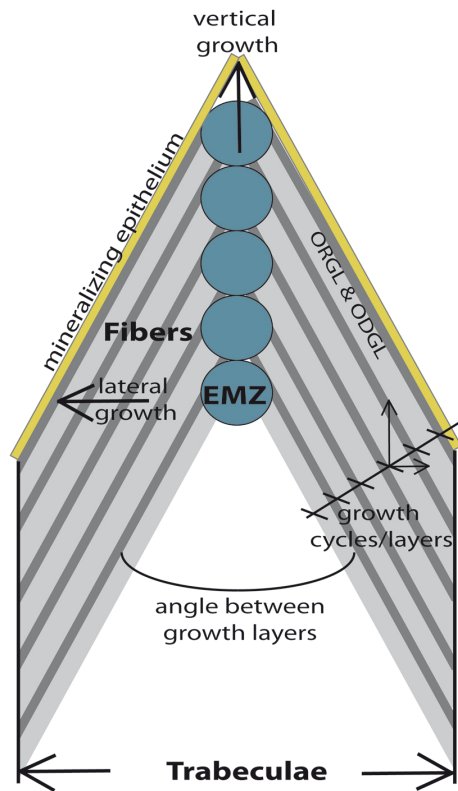


**Fig. 3.** Schematic representation of coral skeletal growth of a trabeculae (modified after Cuif and Dauphin, 2005a). Stepping growth mode of fibers results in growth layers of organic-rich (ORGL, dark grey) and organic-depleted growth lines (ODGL, light grey) to both sides of the early mineralization zone (EMZ). The growth layers are oblique and encompass an angle resulting in differences in vertical and lateral extension per growth cycle.

**Different chemical composition within the skeleton of *Porites lutea***

M. Wall and G. Nehrke

Title Page

Abstract Introduction

Conclusions References

Tables Figures

◀ ▶

◀ ▶

Back Close

Full Screen / Esc

Printer-friendly Version

Interactive Discussion

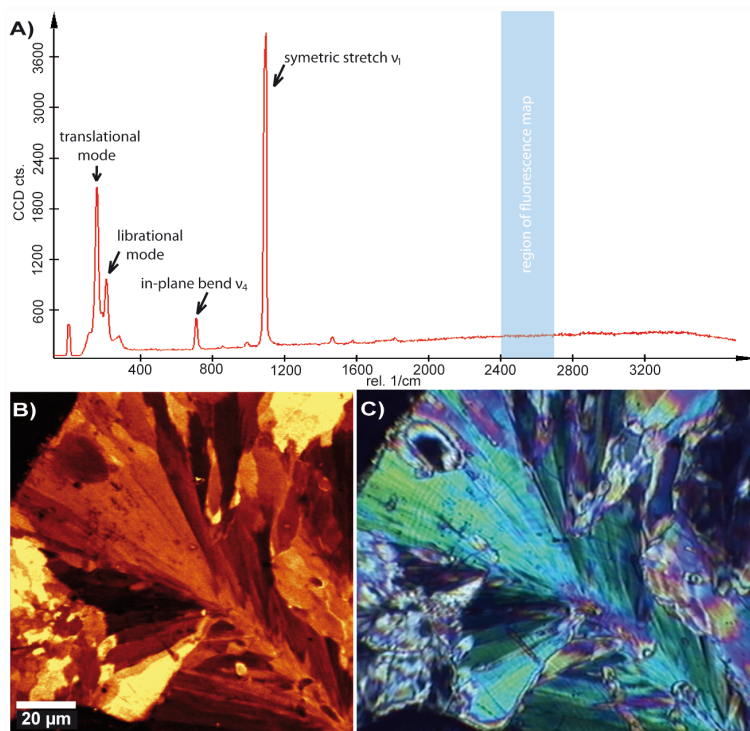


**Fig. 4.** (A) Raman spectra of *Porites lutea* skeleton sample showing the characteristic peaks for aragonite (translational mode at  $155\text{ cm}^{-1}$ , librational mode at  $208\text{ cm}^{-1}$ , in-plane band at  $710\text{ cm}^{-1}$  and symmetric stretch at  $1085\text{ cm}^{-1}$ ). Highlighted in blue is the spectral region used to derive the fluorescence maps. (B) Crystallographic orientation derived from symmetric stretch resembles the fiber orientation in polarized light microscopy (C). (#22\_29MW\_#1, integration time of 0.5 s and 10 accumulations, 100x Nikon Objective).

Different chemical composition within the skeleton of *Porites lutea*

M. Wall and G. Nehrke

Title Page

Abstract

Introduction

Conclusions

References

Tables

Figures

⏪

⏩

◀

▶

Back

Close

Full Screen / Esc

Printer-friendly Version

Interactive Discussion

## Different chemical composition within the skeleton of *Porites lutea*

M. Wall and G. Nehrke

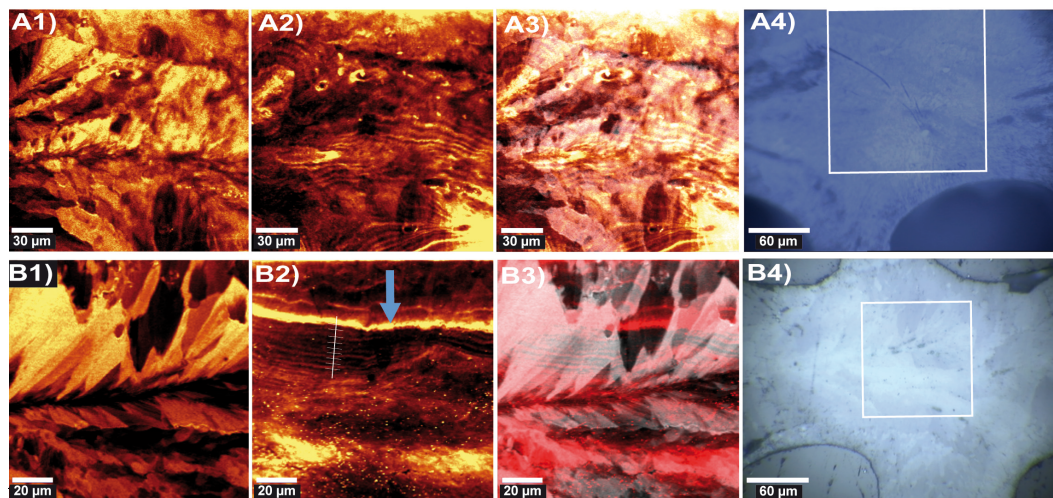


**Fig. 5.** Raman maps of longitudinal non-embedded (**A**; #10\_29MW\_#1) and embedded (**B**; #40\_29MW\_#1) thick sections of *Porites lutea* (Milne Edwards and Haime, 1860). (**A4–B4**) Reflected light images with insert showing the location of the Raman maps. The number of each Raman map (from sample **A** and **B**) indicates the spectral region used for mapping: **(1)** represents the intensity distribution of the symmetric stretch of aragonite ( $1085\text{ cm}^{-1}$ ), **(2)** the fluorescence intensity distribution within the area and **(3)** shows the superposition of map **(1)** and **(2)**. Blue arrows indicate repeated features of organic-rich growth lines (ORGL 2) of increased fluorescence detected within fluorescence maps. The scale bar within fluorescence maps displays the skeletal extension for each growth cycle comprised of one high and one low fluorescence growth line. (Superimposed images derive from WITecProject software).

Title Page

Abstract

Introduction

Conclusions

References

Tables

Figures

◀

▶

◀

▶

Back

Close

Full Screen / Esc

Printer-friendly Version

Interactive Discussion

## Different chemical composition within the skeleton of *Porites lutea*

M. Wall and G. Nehrke

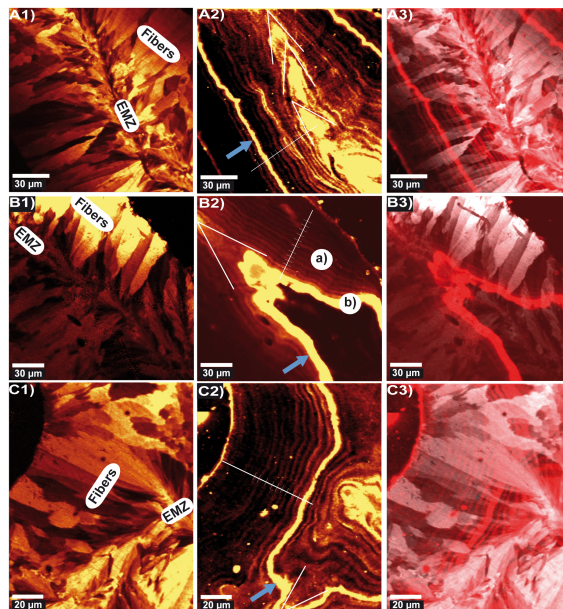


**Fig. 6.** (A–C) Raman maps of *Porites lutea* (Milne Edwards and Haime, 1860) skeleton elements in longitudinal thin section (#22.29MW.#2–4). Numbers indicate the spectra region used for the maps: **(1)** represents the intensity distribution of the symmetric stretch of aragonite ( $1085\text{ cm}^{-1}$ ), **(2)** the fluorescence intensity distribution and **(3)** shows the superposition of map **(1)** and **(2)**. Blue arrows indicate repeated features of organic-rich growth lines (ORGL 2) of increased fluorescence detected within fluorescence maps. White arrow heads represent the oblique traces of the position of mineralizing epithelium forming layered growth increments with a high and a low fluorescence growth line comprising one growth cycle. The scale bar within fluorescence maps displays the skeletal extension for each growth cycle. The two types of growth lines within fluorescence map are indicated in **(B2)** with **(a)** representing the incremental growth layers (organic-rich and organic-depleted growth lines) and **(b)** the high fluorescence growth lines (ORGL 2). (Superimposed images derive from WITecProject software).

Title Page

Abstract

Introduction

Conclusions

References

Tables

Figures

◀

▶

◀

▶

Back

Close

Full Screen / Esc

Printer-friendly Version

Interactive Discussion

## Different chemical composition within the skeleton of *Porites lutea*

M. Wall and G. Nehrke

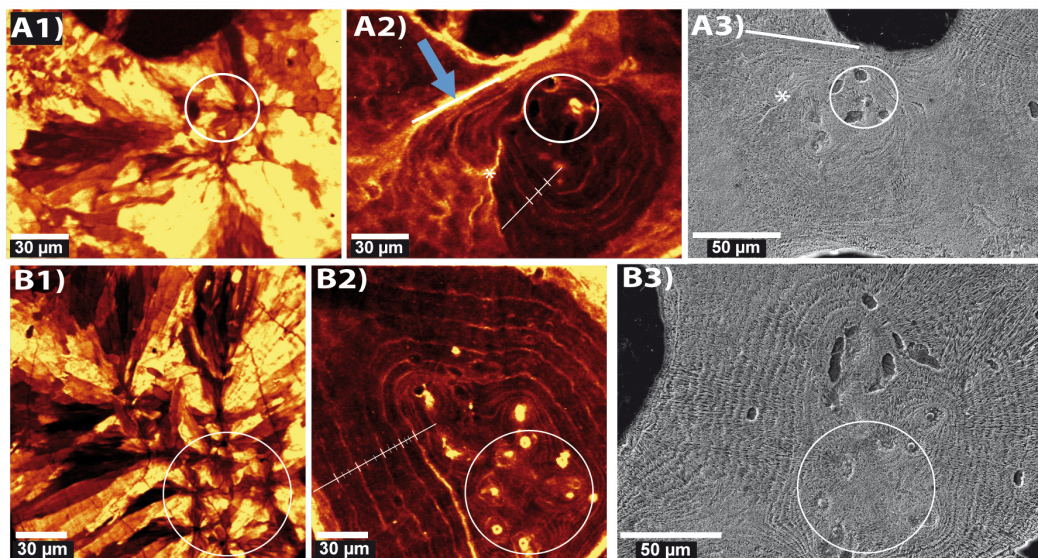


**Fig. 7.** Raman maps of transversal thin section represent the intensity distribution of the symmetric stretch of aragonite ( $1085\text{ cm}^{-1}$ , **A1**, **B1**) and the fluorescence intensity distribution (**A2**, **B2**). (**A3**, **B3**) Scanning electron microscopic images were obtained after Raman mapping and etching of sample (**A**: #20\_29MW\_#1, **B**: #20\_29MW\_#2). Circle in the images illustrates same areas within the different maps for each row. Blue arrows indicate repeated features of organic-rich growth lines (ORGL 2) of increased fluorescence detected within fluorescence maps. The scale bar within fluorescence maps displays the skeletal extension for each growth cycle comprised of one high and one low fluorescence growth lines. Asterisk indicates same regions within the same row of maps.

Title Page

Abstract

Introduction

Conclusions

References

Tables

Figures

⏪

⏩

◀

▶

Back

Close

Full Screen / Esc

Printer-friendly Version

Interactive Discussion

## Different chemical composition within the skeleton of *Porites lutea*

M. Wall and G. Nehrke

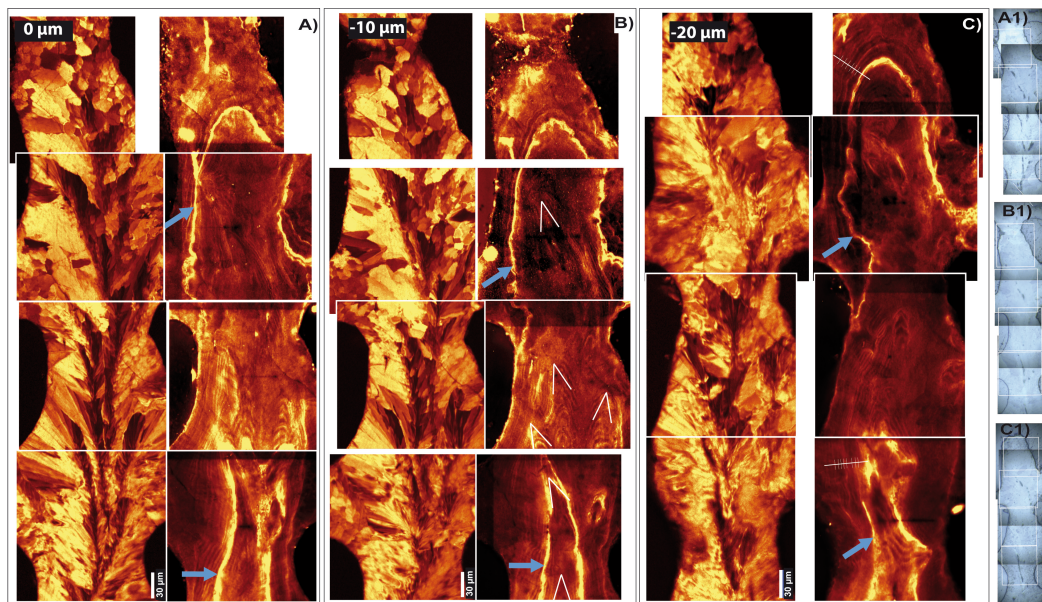


**Fig. 8.** (A–C) Raman maps per depth level (A: 0  $\mu\text{m}$ , B: –10  $\mu\text{m}$  and C: –20  $\mu\text{m}$ ; #40\_29MW\_#2–4) of intensity distribution of the symmetric stretch of aragonite and of fluorescence are plotted on the left and right, respectively. Reflected light images are displayed on the right for each mapped depth layer (A1: 0  $\mu\text{m}$ , B1: –10  $\mu\text{m}$ , C1: –20  $\mu\text{m}$ ). Blue arrows indicate repeated features of organic-rich growth lines (ORGL 2) of increased fluorescence detected within fluorescence maps. White arrow heads represent the oblique traces of the position of mineralizing epithelium forming layered growth increments with a high and a low fluorescence growth line comprising one growth cycle. The scale bar within fluorescence maps displays the skeletal extension for each growth cycle.

Title Page

Abstract

Introduction

Conclusions

References

Tables

Figures

◀

▶

◀

▶

Back

Close

Full Screen / Esc

Printer-friendly Version

Interactive Discussion

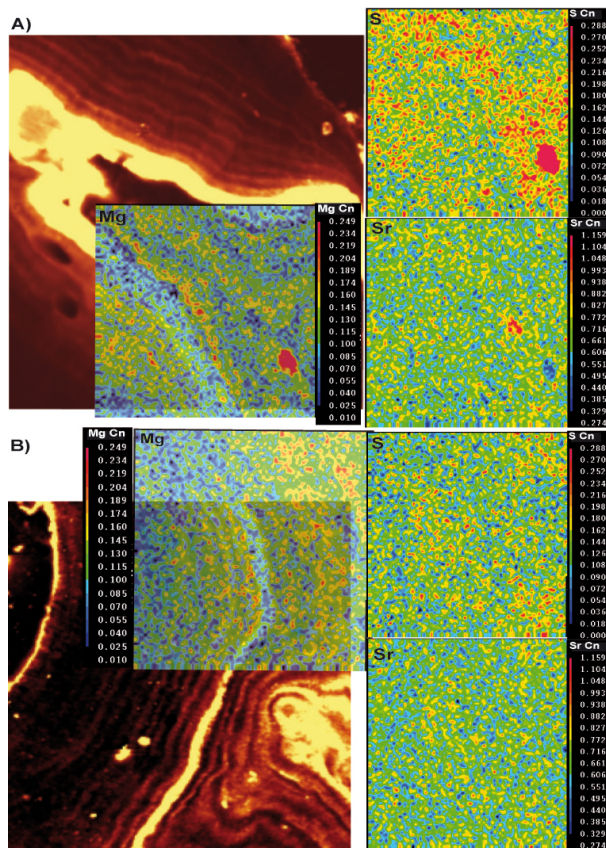


**Fig. 9.** Trace element concentrations (Mg, S, Sr) were mapped with electron microprobe. Mg distribution of the mapped area was superimposed on the respective fluorescence intensity distribution map derived from Raman mapping (**A**: Fig. 3b2, #22\_29MW\_#3, **B**: Fig. 3c2, #22\_29MW\_#4). On the right side of the superimposed images (Adobe Photoshop CS4), the trace element maps of S and Sr are displayed.

**Different chemical composition within the skeleton of *Porites lutea***

M. Wall and G. Nehrke

Title Page

Abstract Introduction

Conclusions References

Tables Figures

◀ ▶

◀ ▶

Back Close

Full Screen / Esc

Printer-friendly Version

Interactive Discussion



## Different chemical composition within the skeleton of *Porites lutea*

M. Wall and G. Nehrke

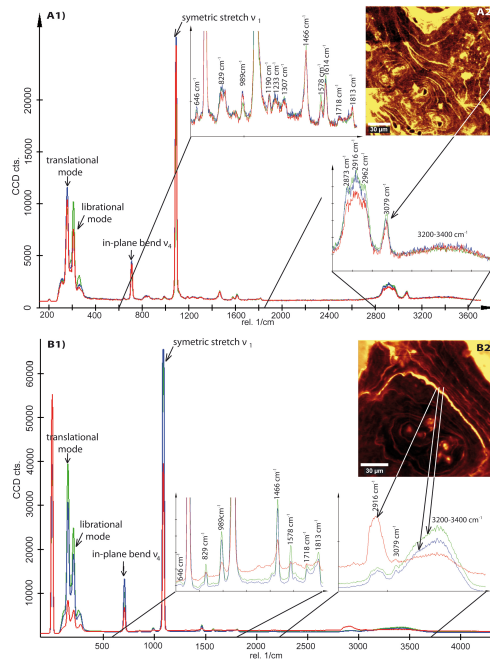


**Fig. 11.** Raman spectra of *Porites lutea* (Milne Edwards and Haime, 1860) skeleton sample (**A**: #20\_29MW\_#3, **B**: #20\_29MW\_#4) showing the characteristic peaks for aragonite (translational mode at  $155\text{ cm}^{-1}$ , librational mode at  $208\text{ cm}^{-1}$ , in-plane band at  $710\text{ cm}^{-1}$  and symmetric stretch at  $1085\text{ cm}^{-1}$ ). Regions of minor peaks are zoomed out:  $600\text{--}1850\text{ cm}^{-1}$  and  $2800\text{--}3600\text{ cm}^{-1}$ . Raman spectra were obtained after mapping the region marked in the fluorescence map in (**A2**) and (**B2**) with following settings for (**A1**)  $532\text{ nm}$  laser wavelength, centered at  $2000\text{ cm}^{-1}$ , integration time of  $0.5\text{ s}$  and 10 accumulations,  $100\times$  Nikon Objective, Analysator set  $90^\circ$  to laser wavelength and (**B1**)  $488\text{ nm}$  laser wavelength, centered at  $2400\text{ cm}^{-1}$ , integration time of  $6\text{ s}$  and 10 accumulations,  $100\times$  Nikon Objective. (Raman spectra were derived in different points and displayed by different colors).

Title Page

Abstract

Introduction

Conclusions

References

Tables

Figures

⏪

⏩

◀

▶

Back

Close

Full Screen / Esc

Printer-friendly Version

Interactive Discussion